Progress In Electromagnetics Research C, Vol. 153, 179–188, 2025

PIER C

(Received 1 January 2025, Accepted 17 February 2025, Scheduled 12 March 2025)

Meta-Surfaces Based High Gain Wide-Band Stacked Antenna with Low Cross-Polarization and Side Lobe Level for 5G Applications

Anjali Rochkari[1], Vijaypal Yadav[2], Mahadu Trimukhe[3], Nayana Chaskar[4], Meenakshi Awasthi[2], and Rajiv Gupta[1,*]

[1]*Department of Electronics and Telecommunication, Terna Engineering College, Navi Mumbai, India*
[2]*Department of Electrical, Electronics and Communication Engineering, Galgotia University, India*
[3]*Bharati Vidyapeeth (Deemed to be University), DET (Off Campus), Navi Mumbai, India*
[4]*M.H. Saboo Siddik College of Engineering, Mumbai, India*

ABSTRACT: This paper proposes a high gain wide band stacked antenna using multiple meta-surfaces that offers stable radiation patterns with low cross-polarization level (CPL) and side-lobe level (SLL) for 5G applications. The suspended microstrip antenna (SMSA) offers high gain and wide bandwidth, but the radiations from probe feed cause high CPL. SMSA design with meta-surfaces increases the inductive impedance of SMSA; therefore, the substrate height is decreased to increase the capacitance to compensate this inductive impedance. It decreases the cross-polar radiation due to decrease in probe feed length. Meta-surfaces electromagnetically couple with SMSA and enhance the bandwidth of antenna. SMSA with meta-surfaces is placed in a half-wavelength Fabry Perot Cavity (FPC) to enhance the gain of antenna. The proposed antenna offers $S_{11} < -10$ dB, peak gain of 16.4 dBi, SLL < -23 dB and CPL < -23 dB, and front to back lobe ratio (FBR) > 22 dB over 3.3–3.9 GHz. The structure is fabricated and tested. The measured results are close to the simulation ones. The proposed structure based on its radiation characteristics is a suitable candidate for 5G applications.

1. INTRODUCTION

Wireless communication is now a part of our life and has influenced every aspect of human life. 5G technology has further given a boost to wireless communication by providing reliable high data rate with low latency. 5G technology finds applications in every field like medicine, agriculture, education, home automation, automobile, robotics, augmented and virtual reality. Human beings are getting habituated to these wireless systems. If these systems and especially antennas are not designed properly, the undesirable radiations in unintended directions cause interference with other devices. High power undesired radiations are harmful and cause health hazards and biological issues.

The antenna with high gain requires low input power as effective power in desirable direction gets multiplied by the gain of the antenna, but it should have low SLL and CPL to mitigate interference and health hazards. MSA on low permittivity and thick dielectric substrate increase the dimensions of antenna while planar and stack multi-resonator patches result in variation in radiation pattern and poor Signal/Noise ratio (SNR). A suspended MSA provides higher gain and wider bandwidth, but as substrate height increases, cross polarization level (CPL) also increases due to the increase in probe feed length [1].

Gain and bandwidth (BW) enhancement by stacking multiple patches above MSA has been reported [2–4]. Two circular patches are placed above a metallic circular or elliptical MSA [2] to achieve 12.1 dBi peak gain with 55.7% BW. But it has high SLL and CPL. 12.5 dBi average gain is obtained using a double-cavity multi-resonator stack antenna. The antenna offers low CPL but has high SLL [3]. Triangular patches are used to design a broadband high gain stack antenna to obtain 10.8 dBi peak gain, but it has -13.6 dB SLL and 15.8 dB FBR [4].

Meta-surfaces (MSs) such as reactive impedance surface (RIS) or artificial magnetic conductor (AMC) are designed, as they control polarization, phase, magnitude of electromagnetic fields, and therefore, the performance of antenna [5, 6]. A non-zero-index NZI MS lens [7], nonuniform [8] or anisotropic elliptical meta-surface [9] are designed to improve FBR or axial ratio bandwidth of a CP antenna [7–9]. Low profile antenna array using RIS and partially reflective surface (PRS) [10], stacked slotted AMC [11] have been reported. CPL and SLL of a suspended MSA are improved using RIS and multiple meta-surfaces in [12, 13]. However, the structures offer low gain.

FPC antennas with one or multiple PRSs or Frequency Selective Surface (FSS) layers are proposed to improve gain and BW in [14, 15]. High gain wide BW, FPC antenna with complementary FSSs [14] fed by an aperture coupled MSA, and dual-polarized wideband antenna using quad PRS [15] have been reported. Gain BW of FPC antennas is enhanced by using hybrid PRS [16] and electromagnetic band gap (EBG) and truncated superstrate [17]. The structure in [16] is fed by a slotted patch, while 1.0λ profile antenna structure in [17] is fed using a

* Corresponding author: Rajiv Gupta (rajivmind@gmail.com).

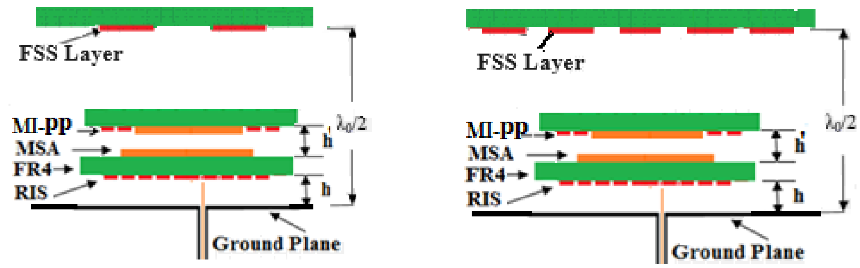

FIGURE 1. FPC antenna with 2×2 (even) and 5×5 (odd) square PP array as FSS layer.

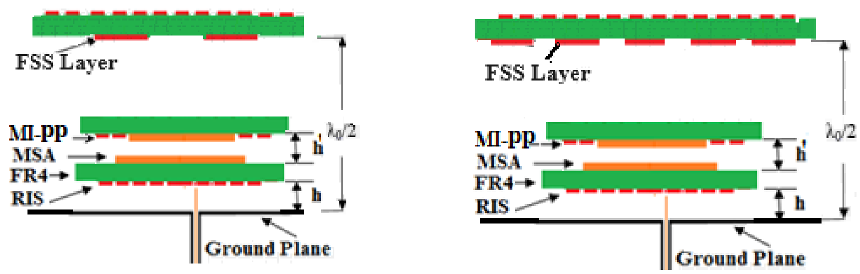

FIGURE 2. FPC antenna with 2×2 (even) and 5×5 (odd) square PP array with AMC as FSS layer.

waveguide attached to a slotted ground plane. These antennas have high SLL. An FPC antenna designed using a superstrate having parasitic hybrid rings as PRS and fed by a holed patch is proposed in [18]. High gain FPC antennas by shaping ground plane [19] and modifying PRS and AMC layers [20, 21] have been investigated. However, high SLL and CPL and feeding difficulties are the drawbacks of these structures.

To mitigate these drawbacks, a novel high gain wideband antenna using multiple meta-surfaces is proposed which provides 16.4 dBi peak gain with low SLL and CPL < -23 dB and > 22 dB FBR, and operates over 3.3–3.9 GHz for 5G applications. The antenna is low in cost, compact, and also easy to fabricate and feed. The architecture of the paper is organized as follows: Antenna geometry with design theory is discussed in Section 2 while Section 3 deals with the simulation results and analysis. Fabrication and measurement results are presented in Section 4 followed by the comparison with state of art antennas in Section 5 and conclusion in Section 6.

2. ANTENNA GEOMETRY AND DESIGN THEORY

The structures shown in Fig. 1 and Fig. 2 consist of a ground plane, feed antenna, and an FSS to form an FPC antenna. Feed antenna consists of a stack SMSA with multiple meta-surfaces. The meta-surface — (a) RIS increases the inductance, reduces the surface waves, and improves impedance matching while (b) the meta-material inspired parasitic patch (MI-PP) increases not only the inductance but also bandwidth (BW), and the whole structure acts as a stack multi-resonator antenna. The increase in inductance is compensated by decreasing the height between substrate and ground plane (h) and between MSA and MI-PP (h').

An RIS or AMC layer is an L-C network in which the conducting patch acts as an inductor L_1 while the spacing between patches is equivalent to a capacitor C_1. Suspended MSA acts

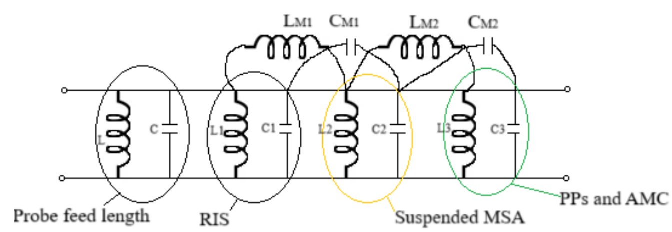

FIGURE 3. Equivalent circuit of stack MSA with meta-surfaces.

as an L_2-C_2 network. The probe feed, a shorted transmission line, acts as an inductor 'L' while the spacing between RIS and ground plane acts as a capacitor 'C'. Slots in AMC layer decreases the inductance and capacitance of the layer. A metallic parasitic patch placed in this slot (PP and AMC or MI-PP) increases the inductance L3 and capacitance C3. The spacing between MSA and PP and AMC acts as a capacitance. The equivalent circuit of stack MSA with meta-surfaces is shown in Fig. 3 [11]. The electromagnetic couplings between RIS and suspended MSA and between MSA and MI-PP are represented by L_{M1} and C_{M1} and L_{M2} and C_{M2}, respectively. Impedance matching can be achieved by increasing inductance due to PP and AMC and RIS, then compensating the increased inductance by increasing capacitance by decreasing the substrate height and spacing between MSA and PP and AMC layers. PP and MSA dimensions are decreased so that antenna operates over 3.3–3.8 GHz.

The FSS consists of an array of PP fabricated on a superstrate with and without a metasurface. The FSS is placed at about $\lambda_0/2$ from the ground plane to form FPC. The dimension and periodicity of square patches of meta-material surface are $< 0.1\lambda_0$, while dimensions of square patches of FSS array are about $\lambda/2$, and the periodicity is about λ. Here, λ_0 and λ are the wavelengths in free-space and dielectric-medium respectively at the central frequency of the operating band.

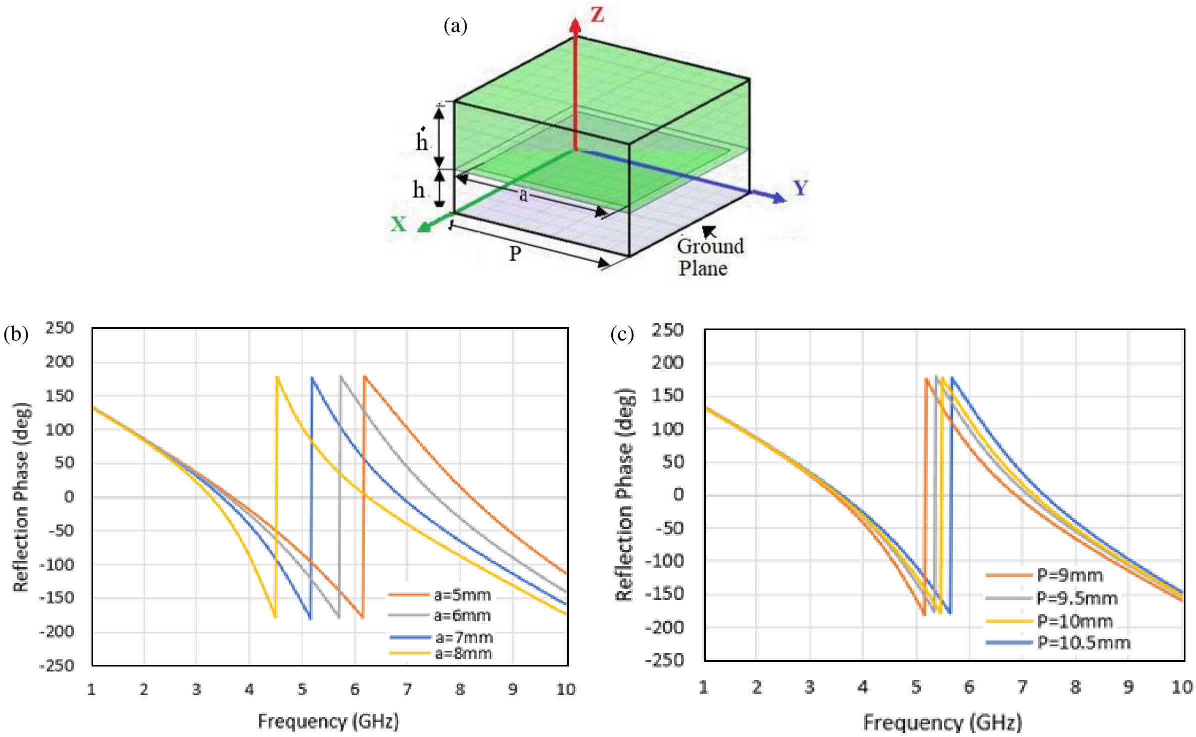

FIGURE 4. Full wave Floquet analysis of periodic structure. (a) Unit cell $h = 3.5$ mm, $h' = 1.59$ mm, $a = 7$ mm, $P = 9$ mm. (b) Effect of patch dimension. (c) Effect of periodicity.

The gain and radiation characteristics of FPC antenna depend on feed antenna; therefore, the antenna feeding the FPC should have low SLL and CPL. Stack SMSA on RIS backed substrate using multiple meta-material is used to feed the FPC as it has low CPL and SLL. RIS improves the impedance bandwidth as it decreases the surface waves by decreasing the interaction between substrate and ground plane. The fields get reflected from RIS and thus contribute to radiation which result in the increase in gain and antenna efficiency [10, 11]. Meta-surface, viz. RIS and meta-material inspired parasitic patch (MI-PP), increases the inductive impedance of the structure which is compensated by decreasing the substrate height or probe feed length. It leads to the decrease in CPL due to the decrease in radiation from probe feed [12, 13].

Gain can be enhanced by fabricating a parasitic patch (PP) or an array of PPs on a dielectric superstrate layer. These metallic PPs enhance the reflection coefficient of PRS and antenna gain. For high directivity or gain, the waves emanating from the PRS must be co-phasal. Therefore, the antenna gain depends on dimensions and spacing between PPs as field amplitude and phase change with dimensions and spacing between PPs fabricated on a superstrate layer. Partially reflecting surface (PRS) used in FPC is designed without and with AMC layer. The dimensions of PPs of FSS are decreased as its distance from feed antenna increases to compensate the phase leg due to the increase in feed path length due to increase in feed path length in comparison to central PP. Further, the PPs are fabricated with unequal spacing to increase the PRS reflection coefficient and the gain of antenna [20, 21].

The antenna feeding the FPC should have wide BW, low SLL and CPL. FPC is a resonant cavity, and therefore, the gain and radiation pattern of FPC depend on frequency. There are several techniques adopted in literature to enhance the BW of FPC antenna, but the radiation pattern varies over large BW [20–24]. In the literature, the work is mainly concentrated on the design of PRS, but in our design, we have designed a feed structure with low SLL and CPL, which resulted in the gain enchantment of FPC antenna with low SLL and CPL over 3.3–3.6 GHz/3.3–3.8 GHz, 5G band. The side view of these configurations without and with AMC are shown in Fig. 1 and Fig. 2, respectively. The design steps in designing the proposed antenna are as follows:

1. Design an SMSA on an FR4 substrate and suspend it above the metallic ground plane to resonate at 3.45 GHz and to operate over 3.3–3.6 GHz using standard design equations [1–3]. Optimize SMSA dimensions and substrate height.
2. Design of RIS and AMC unit cell — Full wave Floquet analysis of periodic structure composed of AMC and RIS is carried out with the help of unit cell, as shown in Fig. 4. $h' = 1.59$ mm FR4 substrate of $P \times P$ dimensions is suspended in air at 'h' from ground plane. The effect of square patch size and periodicity on resonant frequency corresponding to 0° reflection phase crossing and AMC bandwidth corresponding to ±90° phase variation is carried out using High Frequency Structure Simulator (HFSS). The resonant frequency decreases with the increase in patch size, when periodicity is fixed and in-

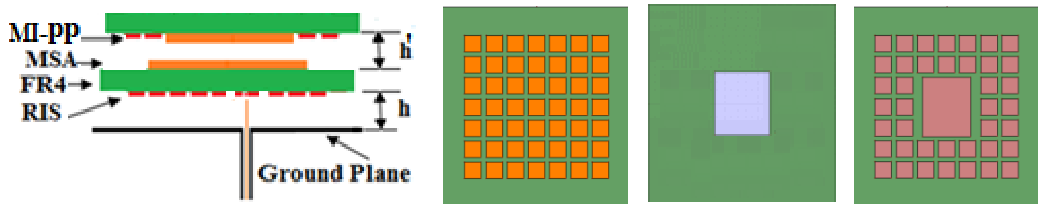

FIGURE 5. Side view of feed antenna along with top view of RIS, MSA, and MI-PP.

creases with periodicity, when patch size is fixed as shown in Fig. 4. Patch dimension of side $a = 7$ mm and periodicity $P = 9$ mm are selected so that resonant frequency is 3.45 GHz, and bandwidth covers the desired impedance bandwidth from 3.3 to 3.8 GHz.

3. Design SMSA on RIS backed FR4 substrate. The RIS consisting of an array of square patches of dimension and periodicity $< 0.1\lambda_0$ is fabricated on the other side of the FR4 substrate of step 1. At 3.45 GHz, $0.1\lambda_0$ is 8.7 mm. So patch dimension is taken as 7 mm with periodicity of 9 mm. The SMSA on RIS backed substrate is designed in [13]. The SMSA dimensions and substrate height are decreased to compensate the inductive impedance of RIS. RIS should extend beyond the SMSA; therefore, RIS consists of 7×7 array of square patches.
4. Design an AMC layer on 1.6 mm FR4 superstrate, similar to RIS, consisting of 7×7 array of square patches of 7 mm side and 9 mm periodicity (dimension and periodicity $< 0.1\lambda_0$) and place above SMSA. The SMSA dimensions and substrate height are decreased to compensate the inductive impedance of AMC. Optimize superstrate and substrate height and dimensions of SMSA to improve BW.
5. Remove the 3×3 array of square patches of AMC, approximately equal to the dimension of SMSA and fabricate a rectangular parasitic patch (PP) to form a stack multi-resonator. PP dimensions should be slightly less than SMSA so that PP resonates at slightly higher frequency than SMSA and electromagnetically couples with SMSA to improve BW. The SMSA dimensions and substrate height are decreased to compensate the inductive impedance of PP. This is the feed antenna of FPC antenna.
6. Design an FSS on an FR4 superstrate consisting of a square PP array (PRS of FPC antenna). The dimensions of patches are about $\lambda/2$, and the spacing between patches is about λ, where λ is the wavelength in dielectric medium at central operating frequency. The patch dimensions and spacing between patches are decreased as its distance from center of feed antenna increases to compensate the phase lag in PP feed and to improve gain by increasing magnitude of reflection coefficient of PRS [20, 21]. Odd array PRS has a patch just above SMSA, while even array PRS does not has a patch just above SMSA.

A rectangular MSA on one side with RIS (an array of square patches of 7 mm side with periodicity of 9 mm) on other side of 1.59 mm FR4 substrate-1 is designed and placed at $h = 1$ mm above the 0.5 mm copper metal ground plane. A second meta-surface (an array of square patches of 7 mm side) is printed on 1.59 mm thick FR4 superstrate-1 around a rectangular parasitic patch (PP), called meta-material inspired PP layer (MI-PP) and placed at h' from substrate-1. FSS layer (an array of square patches) on another 1.59 mm thick FR4 superstrate is designed and placed at about $\lambda_0/2$ from ground plane to form FPC antenna as shown in Fig. 1. The structures in Fig. 2 have another meta-surface AMC formed by an array of square patches of 7 mm with periodicity of 9 mm at the top side of the superstrate. Both dielectric substrate and superstrate have $\varepsilon_r = 4.4$ and $\tan\delta = 0.02$. The suspended MSA is fed using a $50\,\Omega$ coaxial probe. The side view of fed antenna and top views of RIS, MSA, and MI-PP are shown in Fig. 5. The evolution of the FPC structures and related theory are described below.

3. SIMULATION RESULTS AND ANALYSIS

An SMSA is designed on an RIS backed 1.59 mm FR4 substrate (RIS layer — 7×7 array of 7 mm square patches with periodicity of 9 mm), on $80 \times 85\,\text{mm}^2$ ground plane. Now a $26.5\,\text{mm} \times 29.1\,\text{mm}$ parasitic patch (PP) is fabricated on one side of the FR4 superstrate with an array of 7 mm square patches around the PP and placed above SMSA (Fig. 5). The structure is termed as 'Feed Antenna' (FA). $S_{11} < -10$ dB is obtained over 3.3–3.6 GHz. The optimized structure offers 8.6 dBi peak gain. The FBR is about 20 dB and CPL > -18 dB [13]. FA is now placed in FPC to enhance the gain and BW. The structures are simulated using IE3D 15.0 version software.

3.1. Even Array

Initially, a 1.59 mm FR4 superstrate is placed above the FA. Thereafter, 2×2 and 4×4 arrays of square PPs are fabricated on one side of the superstrate called PRS layer, and on the other side the AMC layer consisting of an array of square patches of side 7 mm and periodicity 9 mm is fabricated. The square patches of 21 mm and spacing of 44 mm form the 2×2 array. In even array, there is no metallic patch at the center just above the SMSA (Fig. 2). In 4×4 array of square PPs, central square patches are of 21 mm while outer square patches are 20 mm. The spacing is 44 mm between the center patches and 42 mm between the center patches and outer patches. PRS height is about $\lambda_0/2$. If PRS is capacitive, it is more than $\lambda_0/2$, and if inductive it is less than $\lambda_0/2$. A dielectric PRS is capacitive, therefore its height from the ground plane is about $0.6\lambda_0$. PRS height decreases to $0.55\lambda_0$ when PRS with 2×2 square patches and $0.53\lambda_0$ with 4×4 square patches with meta-material are designed. PRS height also depends on the feed antenna structure. S_{11} and impedance variation of the structures are shown

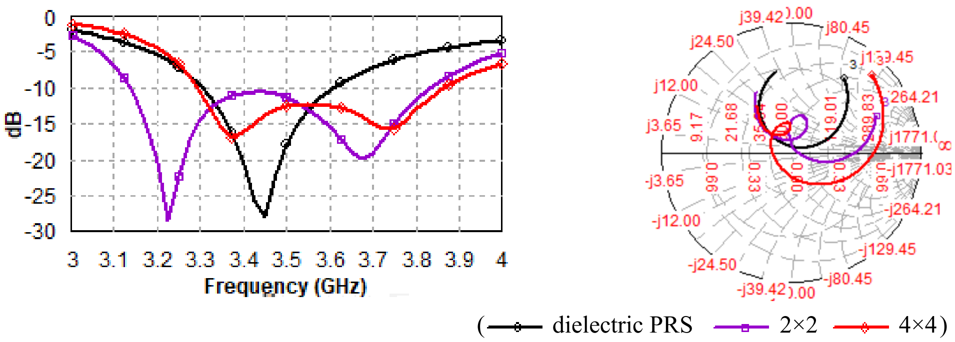

FIGURE 6. S_{11} and impedance variation.

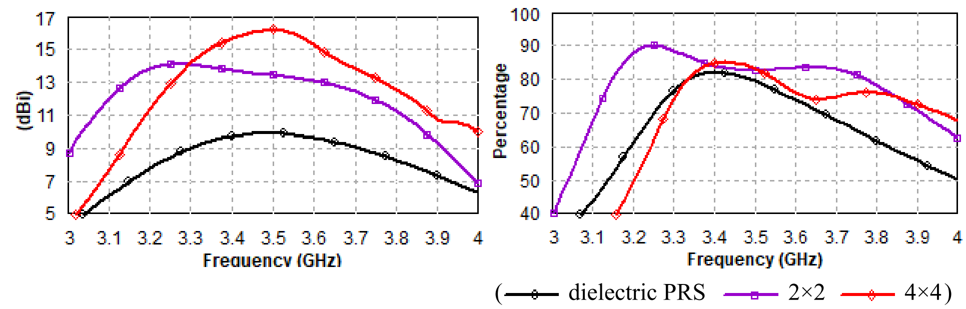

FIGURE 7. Gain and antenna efficiency.

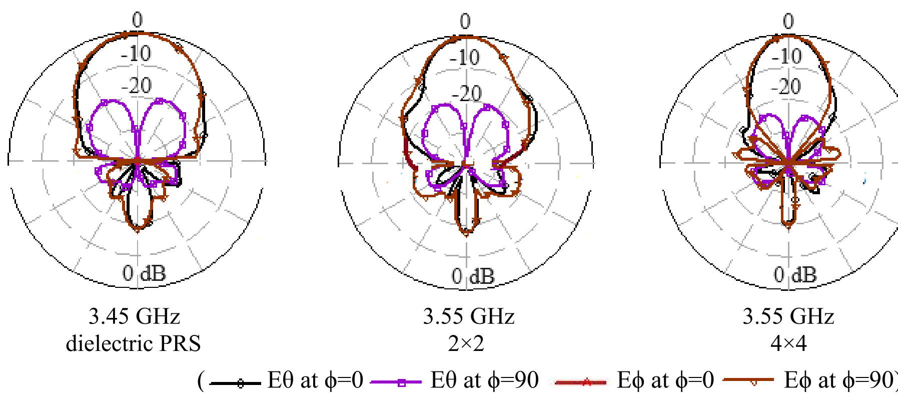

FIGURE 8. Radiation patterns of antenna with even array PRS.

in Fig. 6. A resonant cavity has different parts, viz. PRS, dimension and spacing between square patches of PRS, height of cavity from ground plane, feed antenna consisting of RIS layer, MSA, MI-PP, and meta-material layer. They have their own resonant frequencies. If different parts resonate at different frequencies but close to each other, it gives rise to a wide band as in the case of PRS with 2×2 and 4×4 PP arrays.

The gain of FPC antenna also depends on the resonance of different parts of FPC. If all the parts resonate in unison or near unison, it results in high gain but narrow bandwidth, whereas if different parts resonate at different but nearby frequencies, it results in broadband but moderate gain. Gain and efficiency of structures with different PRSs are shown in Fig. 7. The antenna with a 2×2 array PRS offers $S_{11} < -10$ dB over 3.13–3.80 GHz. It provides wide BW. However, the structure has moderate gain which decreases at higher frequencies. Also antenna efficiency decreases due to degradation in impedance matching at higher frequencies. The antenna with a 4×4 array PRS offers $S_{11} < -10$ dB over 3.3–3.88 GHz. It offers a peak gain of 16 dBi and antenna efficiency $> 70\%$ over the operating band. The radiation patterns of antenna with dielectric PRS at 3.45 GHz (central frequency of 3.3–3.6 GHz band) and at 3.55 GHz (central frequency of 3.3–3.8 GHz band) in the cases of antenna with 2×2 and 4×4 square patch array PRSs are shown in Fig. 8. The dimensions of PPs are progressively decreased, and the spacing between the square patches is decreased in the antenna with 4×4 square PP array PRS to compensate the phase lag. The patches with dimensions $< \lambda/2$ provide capacitive reactance, and therefore, they provide phase lead to compensate the phase lag in feed to PPs far away from the central patch. The antenna with 4×4 square PP array provides 16.0 dBi peak gain with CPL, SLL > -23 dB, and FBR of 20 dB.

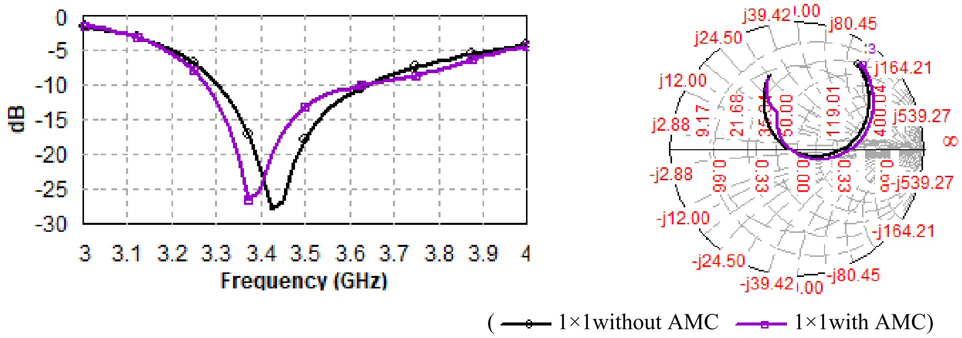

FIGURE 9. S_{11} and impedance variation.

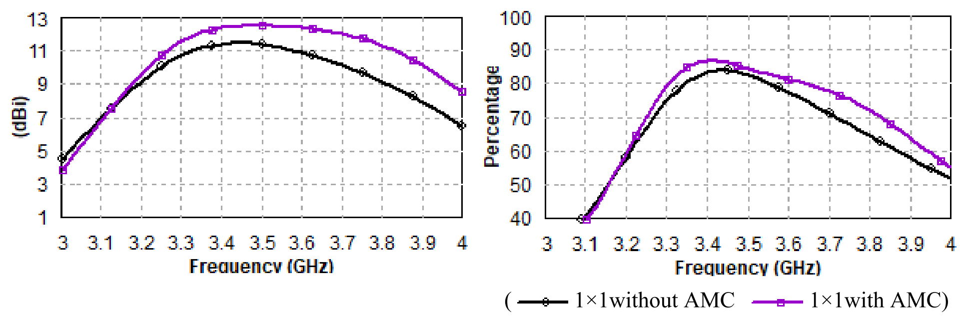

FIGURE 10. Gain and antenna efficiency.

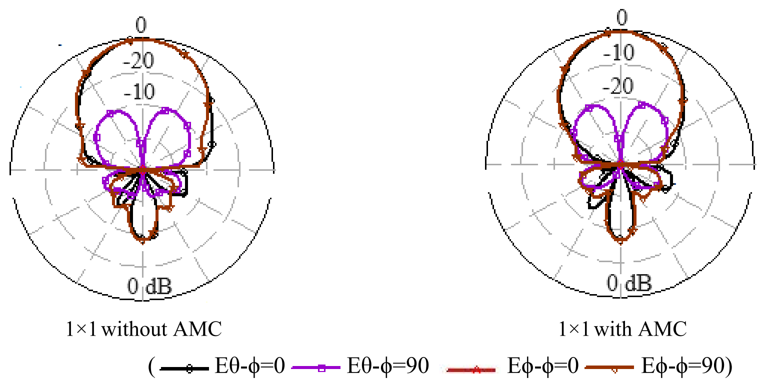

FIGURE 11. Radiation patterns of 1 × 1 without AMC and with AMC antenna.

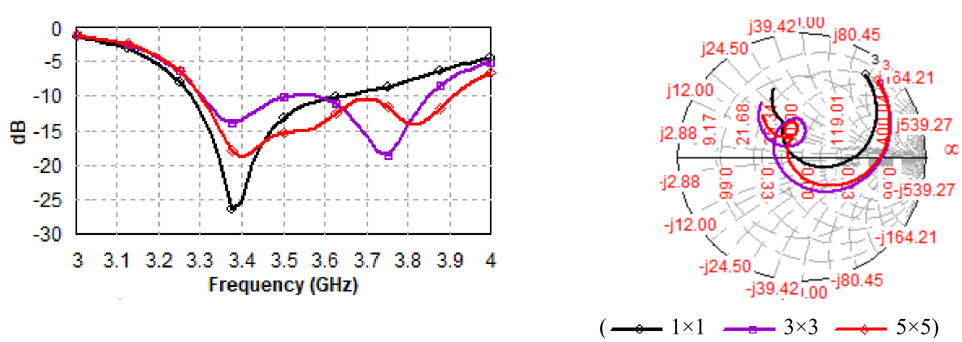

FIGURE 12. S_{11} and impedance variation.

3.2. Odd Array

Structure with 1 × 1 or single metallic patches with and without AMC are designed. 1 × 1 or single metallic patch with AMC provides higher gain than that without AMC. S_{11} and impedance variation, gain and efficiency, and radiation patterns of structures with 1 × 1 metallic patch with and without AMC are shown in Figs. 9, 10, and 11, respectively. Structures with odd 1 × 1, 3 × 3, and 5 × 5 square PP arrays are simulated and

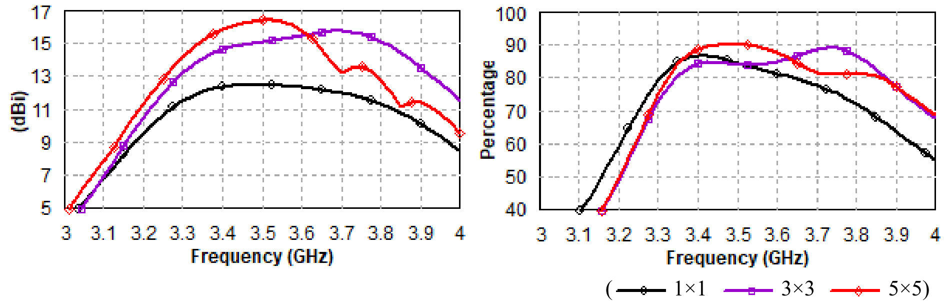

FIGURE 13. Gain and antenna efficiency of odd PP array.

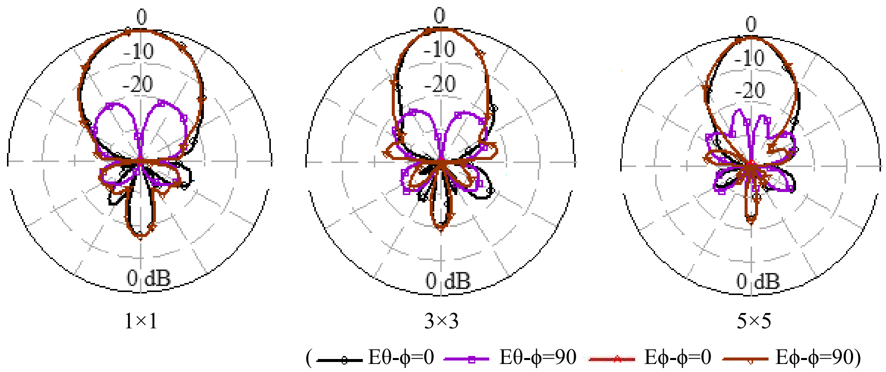

FIGURE 14. Radiation patterns.

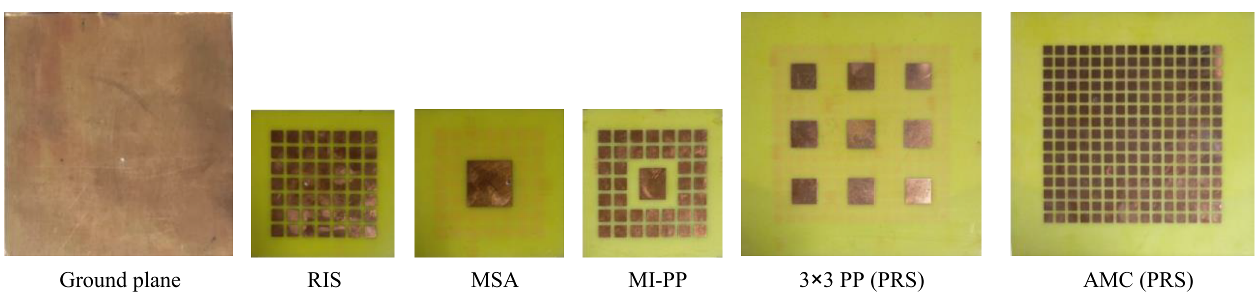

FIGURE 15. Top view of different layers of fabricated antenna.

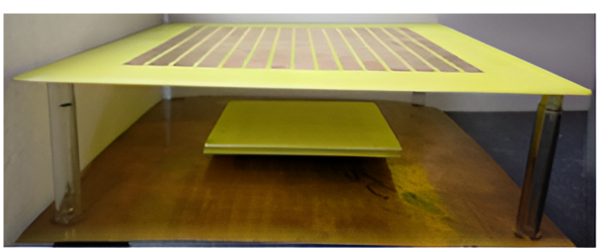

FIGURE 16. 3-dimensional view.

optimized. S_{11} and impedance variation of the structures are shown in Fig. 12. Gain and efficiency of structures with different PRSs are shown in Fig. 13. Radiation patterns of these structures are shown in Fig. 14.

4. FABRICATION AND MEASUREMENT RESULTS

The FPC antenna with 3×3 PP array and AMC as PRS termed as '3×3-array-AMC' is fabricated. The 0.5 mm thick copper metal plate ground plane is precisely cut using LASER technology. The MSA on RIS backed FR4 substrate, MI-PP on FR4 superstrate, and PRS and AMC on another FR4 superstrate are fabricated using photo-lithography technique. Photo-lithography technique employs chemical etching process which removes unwanted metal regions of the metallic layers of FR4 dielectric. Photo-lithography technique provides high accuracy and precise control of the shape and size of the desired pattern. S_{11} and radiation pattern are measured using Agilent Field fox N 9116A network analyzer and standard horn antenna in an anechoic chamber respectively.

The top view of each layer, 3-dimensional view of the antenna, and simulated and measured S_{11} are shown in Figs. 15, 16, and 17, respectively. The simulated and measured gain variations and measured radiation patterns at 3.3 GHz, 3.55 GHz, and 3.8 GHz are shown in Fig. 18 and Fig. 19, respectively.

Radiation patterns are measured in far-field region using standard horn antenna in an anechoic chamber. The standard

TABLE 1. Radiation parameters of the FPC antenna structures.

Antenna Structure with PRS	*Gain (dBi)*	*BW (GHz)*	*SLL (dB)*	*CPL (dB)*	*FBR (dB)*	*Size* ($\lambda_0 \times \lambda_0$)	*Aperture Efficiency %*
Dielectric	10.0	3.3–3.604	−25	−19	19.5	1.48 × 1.48	36.34
1 × 1 array	11.5	3.3–3.65	−24	−20	19	1.48 × 1.48	51.35
1 × 1 array-AMC	12.5	3.28–3.68	−23	−20	17	1.48 × 1.48	64.61
2 × 2 array-AMC	14.1	3.13–3.80	−20	−20	19.5	2.05 × 2.05	48.66
3 × 3 array-AMC	15.8	3.3–3.85	−22	−22	20	2.5 × 2.5	48.41
4 × 4 array-AMC	16.2	3.3–3.88	−23	−23	20	3.0 × 3.0	36.86
5 × 5 array-AMC	16.4	3.3–3.91	−23	−23	22	3.15 × 3.15	35.1

TABLE 2. Comparison of proposed antenna with reported state-of-art antennas (NR-Not Reported).

Ref.	*Gain (dBi)*	*Fractional BW (%)*	*SLL (dB)*	*CPL (dB)*	*FBR (dB)*	*Size* ($\lambda_0 \times \lambda_0 \times \lambda_0$)	*Aperture Efficiency %*
[14]	13.8	26.26	−10	−19	−17	2.4 × 2.4 × 0.5	36.15
[15]	14.7	17.86	−13	−21	−16	1.9 × 1.9 × 0.5	65.05
[16]	17.1	25.38	−8	NR	−16	2.8 × 2.8 × 0.69	52.05
[17]	18.7	17.48	−6	−37	NR	5.0 × 5.0 × 0.75	23.6
[18]	15.8	9.51	−16.4	NR	20	2.35 × 2.35 × 0.63	54.98
[19]	16.0	19.31	−9.5	−13	26	2.75 × 2.75 × 0.56	41.89
[20]	17.4	11.13	−20	−16	20	2.83 × 3.23 × 0.49	47.83
[21]	17.2	11.57	−19	−17	20	2.3 × 2.75 × 0.5	66.02
[22]	10.5	14.77	−17	−15	NR	2.0 × 2.0 × 0.66	22.32
[23]	16.35	4.88	−13	NR	18	2.19 × 2.19 × 0.58	71.59
[24]	10.0	18.87	−5	−10	10	1.0 × 1.0 × 0.5	79.58
This work	16.4	16.92	−23	−23	22	3.15 × 3.15 × 0.5	35.06

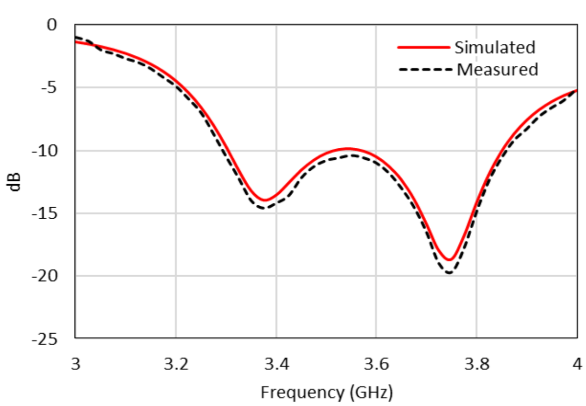

FIGURE 17. Simulated and measured S_{11}.

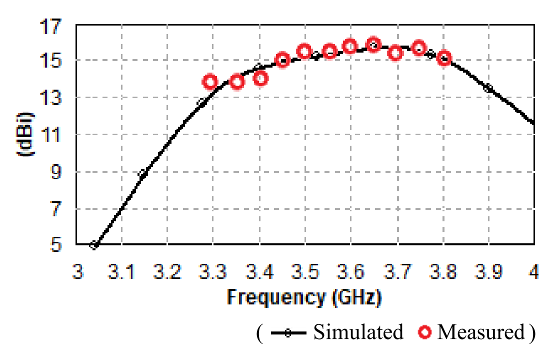

FIGURE 18. Simulated and measured gains.

horn antenna acting as a transmitting antenna is connected to a microwave source, Agilent field fox network analyzer N9916A, and the FPC antenna is connected to Agilent field fox spectrum analyzer. Radiation patterns are measured when transmitting (Tx) and receiving (Rx) antennas are aligned and face each other in E-plane. The receiving antenna is rotated from 0° to 360°. Radiation patterns are also measured when both Tx and Rx antennas are in H-plane. These are co-polar radiation pattern, and SLL is determined from co-polar radiation pattern. When Tx antenna is in E-plane and Rx antenna in H-plane or vice-versa, cross-polar radiation patterns are measured. CPL is determined as the difference between cross-polar maximum value and co-polar maximum value in dB. The gain of antenna is calculated using Friss transmission equation. The cable and connector losses are take into account. The measured results closely align with simulated ones. The slight discrepancy in measured results from simulated ones can be attributed to fabrication error, SMA connector loading, or misalignment of different layers in the prototype antenna. The radiation parameters of different FPC antenna structures are listed in Table 1.

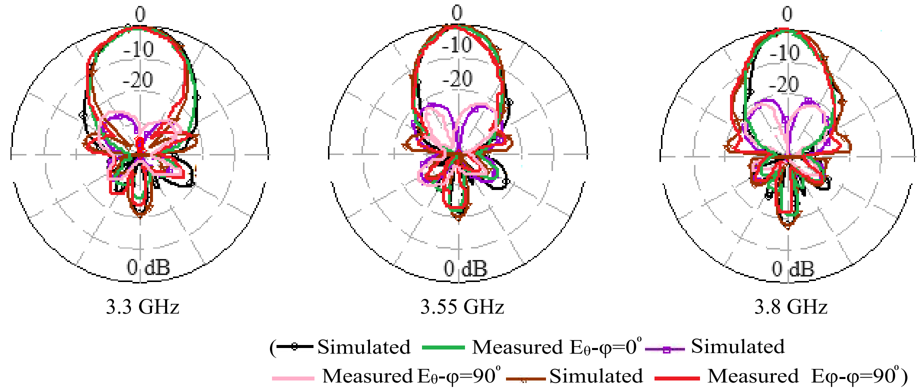

FIGURE 19. Simulated and measured radiation patterns.

Odd array PRS has a parasitic patch just above SMSA, while even array PRS does not have a patch just above SMSA. The gain of FPC antenna depends on the magnitude of reflection coefficient ($|\Gamma|$) of PRS. The FPC antenna with odd array PRS has more gain due to higher $|\Gamma|$ than even array. The effective value of $|\Gamma|$ increases with the increase in array size; as feed antenna has broadside radiation pattern, central patch of FSS intercepts the maximum fields, and the PP away from the central patch intercepts less fields due to the increase in distance [20, 21]. As a result, marginal improvement in gain and aperture efficiency decrease with array size.

5. COMPARISON WITH STATE OF ART FPC ANTENNAS

The proposed antenna is compared with start-of-art antennas reported in the literature in terms of peak gain, % BW, SLL, CPL, FBR, aperture efficiency, and antenna size in Table 2. All the structures have higher SLL and CPL than the proposed antenna except [17] which has lower CPL but significantly higher SLL. The antennas in [14–19, 22, 24] offer large BW, but at the cost of high SLL and CPL. The structures in [16–19, 22] have profile $> 0.5\lambda_0$. The structures in [21, 22] have higher CPL, while antenna in [23] has higher SLL than the proposed antenna. Refs. [15, 16] have higher aperture efficiency but lower FBR and SLL. Refs. [18, 20, 21, 23] have higher aperture efficiency but narrow BW. Antenna in [24] also has higher aperture efficiency but lower gain and FBR. The proposed antenna offers low SLL and CPL, high F/B ratio, and simple design compared to state of art antennas reported in the literature. It is easy to feed and fabricate and has the advantages of low cost, light weight, and planar structure.

6. CONCLUSION

The gain of FPC antenna depends on feed antenna and PRS. FPC fed by an antenna with low CPL and SLL offers gain enhancement over wide BW with low CPL and SLL and high FBR. AMC on PRS helps in reducing the height of FPC and also enhances the gain with improved radiation characteristics. Using this concept, a novel high gain wideband antenna using multiple meta-surfaces is designed that provides 16.4 dBi peak gain with low SLL and CPL < -23 dB and $>$ 22 dB FBR over 3.3–3.9 GHz for 5G applications. The compact low-cost antenna is easy to design, fabricate, and feed. Dual band and circularly polarized antennas with low SLL and CPL may be designed using this concept.

LIST OF ABBREVIATIONS

AMC Artificial magnetic conductor
MI-PP Meta-material inspired parasitic patch
BW Band width
MS Meta-material surface
CP Circularly polarized
MSA Microstrip antenna
CPL Cross polarization level
NZI Non-zero index
SLL Side lobe level
PP Parasitic patch
FA Feed antenna
PRS Partially reflecting surface
FBR Front to back lobe ratio
RIS Reactive impedance surface
FPC Fabry Perot cavity
SMSA Suspended microstrip antenna
FSS Frequency selective surface
SNR Signal to noise ratio

REFERENCES

[1] Kumar, G. and K. P. Ray, *Broadband Microstrip Antennas*, Artech House, Norwood, MA, 2003.
[2] Chopra, R. and G. Kumar, "Broadband and high gain multilayer multiresonator elliptical microstrip antenna," *IET Microwaves, Antennas & Propagation*, Vol. 14, No. 8, 821–829, 2020.
[3] Raha, K. and K. P. Ray, "Broadband high gain and low cross-polarization double cavity-backed stacked microstrip antenna," *IEEE Transactions on Antennas and Propagation*, Vol. 70, No. 7, 5902–5906, 2022.
[4] Chopra, R. and G. Kumar, "High gain broadband stacked triangular microstrip antennas," *Microwave and Optical Technology Letters*, Vol. 62, No. 9, 2881–2888, 2020.

[5] Kumar, P., T. Ali, and M. M. M. Pai, "Electromagnetic metamaterials: A new paradigm of antenna design," *IEEE Access*, Vol. 9, 18 722–18 751, 2021.

[6] Milias, C., R. B. Andersen, P. I. Lazaridis, Z. D. Zaharis, B. Muhammad, J. T. B. Kristensen, A. Mihovska, and D. D. S. Hermansen, "Metamaterial-inspired antennas: A review of the state of the art and future design challenges," *IEEE Access*, Vol. 9, 89 846–89 865, 2021.

[7] Singh, A. K., M. P. Abegaonkar, and S. K. Koul, "Compact near zero index metasurface lens with high aperture efficiency for antenna radiation characteristic enhancement," *IET Microwaves, Antennas & Propagation*, Vol. 13, No. 8, 1248–1254, 2019.

[8] Zheng, Q., C. Guo, J. Ding, and G. A. E. Vandenbosch, "Use of non-uniform RIS and parasitic strips to improve antenna CP performance," *IET Microwaves, Antennas & Propagation*, Vol. 14, No. 14, 1795–1802, 2020.

[9] Srivastava, K., S. Kumar, S. Dwari, B. K. Kanaujia, H. C. Choi, and K. W. Kim, "Anisotropic meta-surface-based wideband high gain circularly polarized patch antenna," *Electromagnetics*, Vol. 40, No. 8, 594–604, 2020.

[10] Jagtap, S., A. Chaudhari, N. Chaskar, S. Kharche, and R. K. Gupta, "A wideband microstrip array design using RIS and PRS layers," *IEEE Antennas and Wireless Propagation Letters*, Vol. 17, No. 3, 509–512, 2018.

[11] Rochkari, A., S. Verulkar, M. Trimukhe, V. Bodade, and R. Gupta, "Low profile high gain wideband stacked MSA array for 5G, WLAN and C-band applications," *International Journal of Microwave & Optical Technology*, Vol. 19, No. 1, 1–9, 2024.

[12] Meng, F., Y. Liu, and S. K. Sharma, "A miniaturized patch antenna with enhanced bandwidth by using reactive impedance surface ground and coplanar parasitic patches," *International Journal of RF and Microwave Computer-Aided Engineering*, Vol. 30, No. 7, e22225, 2020.

[13] Rochkari, A., S. M. Verulkar, N. Chaskar, M. A. Trimukhe, and R. K. Gupta, "Cross polar reduction of a high gain wideband stacked microstrip antenna using metasurfaces," *Progress In Electromagnetics Research Letters*, Vol. 119, 91–98, 2024.

[14] Wang, N., Q. Liu, C. Wu, L. Talbi, Q. Zeng, and J. Xu, "Wideband Fabry-Perot resonator antenna with two complementary FSS layers," *IEEE Transactions on Antennas and Propagation*, Vol. 62, No. 5, 2463–2471, 2014.

[15] Qin, P.-Y., L.-Y. Ji, S.-L. Chen, and Y. J. Guo, "Dual-polarized wideband Fabry-Pérot antenna with quad-layer partially reflective surface," *IEEE Antennas and Wireless Propagation Letters*, Vol. 17, No. 4, 551–554, 2018.

[16] Liu, Z., S. Liu, X. Zhao, X. Kong, Z. Huang, and B. Bian, "Wideband gain enhancement and RCS reduction of Fabry-Perot antenna using hybrid reflection method," *IEEE Transactions on Antennas and Propagation*, Vol. 68, No. 9, 6497–6505, 2020.

[17] Hashmi, R. M. and K. P. Esselle, "Enhancing the performance of EBG resonator antennas by individually truncating the superstructure layers," *IET Microwaves, Antennas & Propagation*, Vol. 10, No. 10, 1048–1055, 2016.

[18] Dang, D.-N. and C. Seo, "Compact high gain resonant cavity antenna with via hole feed patch and hybrid parasitic ring superstrate," *IEEE Access*, Vol. 7, 161 963–161 974, 2019.

[19] Ji, L.-Y., P.-Y. Qin, and Y. J. Guo, "Wideband Fabry-Perot cavity antenna with a shaped ground plane," *IEEE Access*, Vol. 6, 2291–2297, 2017.

[20] Jagtap, S. D., R. K. Gupta, N. Chaskar, S. U. Kharche, and R. Thakare, "Gain and bandwidth enhancement of circularly polarized MSA using PRS and AMC layers," *Progress In Electromagnetics Research C*, Vol. 87, 107–118, 2018.

[21] Chaskar, N., S. D. Jagtap, R. Thakare, and R. K. Gupta, "Gain flattening of wideband FPC antenna using elliptical and rectangular slotted AMC layers," *Progress In Electromagnetics Research C*, Vol. 110, 81–89, 2021.

[22] Vaid, S. and A. Mittal, "Wideband orthogonally polarized resonant cavity antenna with dual layer Jerusalem cross partially reflective surface," *Progress In Electromagnetics Research C*, Vol. 72, 105–113, 2017.

[23] Singh, A. K., M. P. Abegaonkar, and S. K. Koul, "High-gain and high-aperture-efficiency cavity resonator antenna using metamaterial superstrate," *IEEE Antennas and Wireless Propagation Letters*, Vol. 16, No. 6, 2388–2391, 2017.

[24] Guthi, S. and V. Damera, "High gain and wideband circularly polarized S-shaped patch antenna with reactive impedance surface and frequency-selective surface configuration for Wi-Fi and Wi-Max applications," *International Journal of RF and Microwave Computer-Aided Engineering*, Vol. 31, No. 11, e22865, 2021.